NASA-CR-205287

Final Report
for
NASA grant NCC3-189
(KSU # 440224)

"Contact Sensor Attachment to Titanium Metal Composites"

Principal Investigator: Dr. Carlos Vargas-Aburto

SUMMARY

A Pd-13wt%Cr solid solution is a promising high-temperature strain gage alloy. In bulk form it has a number of properties that are desirable in a resistance strain gage material, such as a linear electrical-resistance-versus-temperature curve to 1000 °C and stable electrical resistance in air at 1000 °C. However, unprotected fine wire gages fabricated from this alloy perform well only to 600 °C. At higher temperatures severe oxidation degrades their electrical performance. In this work Auger electron spectroscopy has been used to study the oxidation chemistry of the alloy wires and ribbons. Results indicate that the oxidation is caused by a complex mechanism that is not yet fully understood. As expected, during oxidation, a layer of chromium oxide is formed. This layer, however, forms beneath a layer of metallic palladium. The results of this study have increased the understanding of the oxidation mechanism of Pd-13wt%Cr.

INTRODUCTION

Hypersonic vehicle research and continued improvement of gas turbine engines require more experimental data on the performance of engine and airframe components under harsh conditions. One of the more important parameters requiring measurement is static strain at temperatures to approximately 1000 °C. Measuring static strain at high temperatures with a resistance strain gage requires levels of electrical stability and repeatability that are currently unavailable with commercial gages. However, during a NASA-sponsored program (ref. 1), a solid solution of Pd-13wt%Cr (henceforth called PdCr) has shown promise in overcoming these limitations and extending the range of static strain measurement to higher temperatures.

As a bulk alloy PdCr displays a number of intrinsic characteristics that make it attractive for use in high-temperature strain gages. PdCr has a relatively high melting point of 1397 °C and displays stable electrical resistance in air at 1000 °C. The relationship of electrical resistance to temperature for PdCr is linear to over 1000 °C and, unlike that for many other candidate materials, it is insensitive to heating or cooling rates (ref. 1). Formation of an adherent, self-protective chromium oxide film provides the bulk alloy with good oxidation resistance. In addition, PdCr exhibits strong adhesion to alumina, which provides electrical isolation between the substrate and the sensor material.

Although the bulk alloy has many desirable properties, problems have been observed when PdCr has been fabricated into fine wires and thin films. When this alloy is fabricated into these structures with relatively large surface-to-volume ratios, the alloy's performance degrades at elevated temperatures. When the alloy wires or thin films are heated in air for prolonged times at temperatures above 600 °C, unstable electrical resistance has been observed (ref. 2). This sensor failure problem has been attributed to severe oxidation of the alloy.

In preliminary oxidation studies chemical analyses after annealing above 600 °C in air indicated that the surface chemistry of the wires influenced the electrical properties to a far greater degree than did previously studied larger rod structures (ref. 3). First, palladium has been reported to segregate to the surface rather than a surface layer of chromium oxide being formed (ref. 3). Second, palladium has also been found to be enriched at the grain boundaries following oxidation (ref. 3). Last, aluminum and other trace elements have been reported as contaminants (ref. 4).

In order to understand these chemical differences and to improve the electrical performance of this alloy at high temperatures, a controlled oxidation study has been undertaken and is reported here. Two sample configurations, wire and ribbon, were used for this study. These sample configurations provide relatively high surface-to-volume ratios and thereby simulate an important aspect of strain gages that are currently being designed to be minimally intrusive. The ribbon was also an ideal size for analysis in the spectrometer.

Thermal treatments were conducted in both air and vacuum. Because palladium enrichment and contamination had been observed in the preliminary oxidation studies referenced earlier, the vacuum treatments were included in order to separate the thermally induced effects, such as phase changes, grain growth, and segregation, from the effects due to oxidation.

After the heat treatment the chemistry of each annealed sample was studied by Auger electron spectroscopy (AES). AES elemental maps provided information on the spatial distribution of palladium, chromium, and oxygen. Compositional analysis of the sample as a function of depth was determined by performing argon ion sputter etching and recording a depth profile. The spectroscopic results assisted in suggesting a mechanism for the oxidation process.

During this study an extensive literature search has been completed. A bibliography of all literature sources used in the present investigation is included.

EXPERIMENTAL PROCEDURE

Samples

The samples used for analysis consisted of wires and ribbons fabricated from bulk material with a nominal composition of Pd-13wt%Cr (23 at.% Cr). The material was analyzed by atomic emission spectroscopy for aluminum, copper, iron, platinum, and silicon. The results are presented in the following table:

Element	Content,[a] wt%	
	Wire	Ribbon
Aluminum	<0.001	0.1
Copper	.018	.1
Iron	.085	.1
Platinum	.15	.2
Silicon	.002	.1

[a]Values are from National Spectrographic Laboratories. Sample size limited the relative accuracy to 10%.

Wire samples were 70 μm in diameter. The wire was supplied by Battelle-Columbus Laboratories (Columbus, Ohio) and had been produced by casting, drawing, and then annealing. Ribbon samples were 70 μm thick and 2.5 mm wide. The ribbon was produced at NASA Lewis by a spin melt process that is essentially a quenching process and may incorporate impurities during fabrication. The fine wire was subjected to substantially more cold working and annealing than was the ribbon. The surface-to-volume ratio of the wires was nearly twice that of the ribbons. Even though the wire diameter and the ribbon thickness were substantially greater than in actual strain gages, these configurations were selected in order to facilitate analysis by AES.

The samples were prepared as follows: They were first cleaned in a 1:1 solution of concentrated hydrochloric and nitric acids for 15 s. After chemical etching they were rinsed in deionized water, acetone, and three baths of methanol. After they were dried with nitrogen gas, the samples were handled with degreased tools. Because of the limited supply of these materials the samples were cut into 1- to 2-cm lengths for thermal cycling.

Heat Treatment

Two different heat treatments were completed. The first was under vacuum conditions. The vacuum furnace anneals were done in a diffusion-pumped vacuum chamber at base pressures below 5×10^{-5} Pa. The second set of thermal cycling experiments was done in air using a muffle furnace. For both the vacuum and air anneals the temperatures were monitored with a type K (Chromel-Alumel) thermocouple mounted within 4 cm of the sample and having a calibrated digital readout. The annealing times and temperatures are listed in table I.

Analysis

The chemistry of both preannealed and postannealed samples was analyzed by AES. Each sample was mounted into the spectrometer by clamping under a molybdenum mask. AES surveys, depth profiles, elemental maps, and line scans were obtained with a Perkin-Elmer Model 4300 scanning Auger microprobe (SAM) system. Secondary electron detector (SED) images of analysis areas were also obtained with this system. Mechanical drift of the sample manipulator and an electronics problem with the detector of this spectrometer limited the operating conditions and caused poor signal-to-noise levels. For most of the analyses the primary electron beam voltage was 5 kV and the beam current was generally less than 10 nA.

In order to examine the thicknesses of the surface species and any underlying layers, depth profiles were obtained by argon ion sputtering at 4 kV. During a profile the peak-to-peak intensity of the major Auger transition for each element being investigated was recorded as a function of controlled sputter etching time, which is related to the depth into the sample. Sputtering rates varied from 10 to 90 nm/min as calibrated against a standard of Ta_2O_5/Ta. Atomic concentrations, which are only semiquantitative values, were calculated by using the Perkin-Elmer sensitivity factors (ref. 5).

After the depth profile the resulting crater was imaged. The various layers were readily detected from the SED image. Line scans across the crater edge were recorded to verify the thickness of the layers observed in the depth profile. A line scan is a plot of the peak-to-peak height, which is related to the atomic concentration, as a function of distance.

In addition to the samples already described, a cross section of a PdCr ribbon was prepared for additional AES analysis. The 45-μm-thick PdCr ribbon, which had previously been annealed in air at 800 °C

for 16 hr, was held vertically in an approximately 3-cm-diameter mold and covered with a liquid plastic. After the plastic hardened, it and the ribbon were cut so as to expose a cross section of the ribbon. This cut face was then polished. In order to place the sample in the Auger spectrometer, the plastic mounting material was cut away, reducing the sample size but leaving the polished cross section of the ribbon exposed. By reducing the amount of plastic to be inserted into the spectrometer to the smallest size that would permit handling, outgassing was minimized and the vacuum integrity was maintained throughout the analysis. Approximately 20 nm of gold was sputter deposited on the polished face of the plastic-covered sample, and 100 nm of gold on the other sides, to prevent sample charging and to provide an electrically conducting surface.

RESULTS AND DISCUSSION

Vacuum Anneals

Surface roughness and precipitate formation.—After vacuum annealing two major changes in surface morphology were noted. First, the surface roughness changed. Second, with higher temperature treatments precipitates formed on the surface.

During vacuum annealing significant surface roughness changes were observed on both the ribbons and the wires. The three SED images displayed in figure 1 were recorded of the wire surfaces after 20 hr of annealing at three different temperatures. As the temperature was increased from 550 to 950 °C (figs. 1(a) to (c), respectively), the surface roughness decreased. This decrease in surface roughness with increasing temperature could possibly be due to grain growth, which reduced the number of grain boundaries. No attempt was made in this study to verify grain growth.

The second major morphological change upon vacuum annealing was the formation of precipitates, which can be observed as white dots in figures 1(b) and (c). These precipitates, which were detected only on samples heated above 700 °C, became more noticeable as the annealing temperature increased. The formation of these precipitates with increased annealing temperature suggested the dissolution of impurities and their segregation from the bulk alloy.

Survey scans.—AES data were collected in order to identify the elemental composition of these precipitates and to determine if any segregation had occurred. With the electron beam focused onto a white precipitate on a wire annealed at 800 °C for 20 hr, a survey scan was recorded. The result, shown in figure 2, revealed the presence of aluminum along with palladium and chromium and the other more common surface contaminants sulfur, carbon, and oxygen. Aluminum was detected only in the areas with precipitates. Lei (ref. 3) had previously suggested that aluminum and silicon may cause microstructural transitions in an alloy wire annealed above 800 °C. The origin of the aluminum was not positively identified, but it could be a processing impurity that upon heating segregated to the alloy surface.

An AES survey scan of a featureless area of a wire annealed at 1000 °C for 20 hr (fig. 3) revealed similar surface contaminants of sulfur, carbon, and oxygen but no aluminum. From the peak intensities for the palladium MNN transition at 330 eV and for the chromium LMM transition at 490 eV, approximate atomic concentrations of 40% palladium and 21% chromium were determined, with the balance consisting of 4% sulfur, 20% oxygen, and 15% carbon. Because the ratio of the chromium concentration to the palladium concentration was higher than in the bulk alloy and oxygen was present, chromium oxide enrichment at the surface was theorized.

Depth profiles.—In order to determine whether the sulfur, carbon, and chlorine were only surface contaminants, a depth profile of a ribbon annealed in vacuum at 650 °C for 20 hr was obtained (fig. 4). In this profile the sulfur, carbon, and chlorine were etched away in the first several minutes of sputter time. These results suggested that sulfur, carbon, and chlorine were only surface contaminants, and therefore their spectral lines were deleted during data processing in order to eliminate interference with overlapping lines for the three major elements being investigated in this study. The two zero units on the x axis represented *two* presputter cycles. A single cycle consists of recording several sweeps over the elemental peak for all the elements to be investigated. Two presputter cycles were recorded in order to establish initial atomic concentration values. From the initial values the ratio of the chromium concentration to the palladium concentration was found to be higher on the surface than in the bulk alloy. The bulk composition was reached after a single cycle of sputter etching. The oxygen level observed in the remainder of the profile was essentially the noise level and did not represent oxygen in the bulk. In fact, upon examination of the spectral data for the oxygen region, no oxygen peak was detected after approximately 10 nm of the surface had been removed.

These vacuum annealing studies also suggested that no major alloy degradation due to segregation of palladium or chromium had occurred. The most significant segregating element was aluminum (an impurity), which formed precipitates. The precipitates were assumed to be primarily at the surface because none were detected when the sputter crater was examined and SED images of the crater were recorded.

A small amount of oxidation may have been present on the wire annealed at 950 °C for 20 hr. A depth profile on this wire (fig. 5) indicated that a 20-nm-thick, oxide-rich, palladium-deficient layer (point B to point C) began about 20 nm beneath the surface. This thin layer was probably associated with a small amount of oxidation caused by residual oxygen in the vacuum furnace where the anneals were done. A layered structure, with palladium on top and oxide beneath, was seen in the air anneals and is discussed in the following section.

Air Anneals

Surface roughness.—Upon examination of SED micrographs the samples annealed in air were found to be much rougher than the samples annealed in vacuum. In fact, the roughness of the air-annealed samples was of such a magnitude that any precipitates, such as those detected after vacuum annealing, would have been indistinguishable from the rough scale. As shown in figure 6 the topography of wires annealed for 20 hr in air at 550, 750, and 800 °C increased in roughness both with increasing temperature and relative to the vacuum-annealed counterparts. This increased surface roughness after air annealing was particularly pronounced in the samples annealed at or above 750 °C. The vacuum-annealed sample (fig. 1(b)) began to get significantly smoother at 750 °C, whereas the air-annealed surface in figure 6(b) was substantially rougher.

Below 800 °C, ridges (believed to be located over grain boundaries) were visible on the samples (figs. 6(a) and (b)). At 800 °C and above, the surface of the wires appeared to be covered by a thick scale containing a few holes (fig. 6(c)).

Survey scans.—AES survey scans recorded on samples after annealing in air revealed high concentrations of palladium on the surfaces. Figure 7 shows a survey scan of a wire annealed in air for 5 hr at 850 °C. The spectrum was dominated by strong palladium lines. The weaker palladium peak at 279 eV was severely overlapped by the carbon KLL transition. Peaks from oxygen and carbon are believed to be due to a few monolayers of surface contamination, which are commonly observed on samples exposed to room air.

Depth profiles.—Depth profiles on air-annealed samples indicated that the palladium-rich layer covered an oxide-rich layer. Figure 8 shows a depth profile of a wire annealed in air for 20 hr at 600 °C. The two presputter data acquisition cycles revealed palladium and oxygen with only a small amount of chromium at the surface. The oxygen concentration dropped to near the noise level almost immediately upon sputtering. This behavior was consistent with the hypothesis that the oxygen detected in figure 7 was only surface contamination due to exposure to room air. After this surface contamination was removed, a palladium-rich layer was exposed. From point A to point B in figure 8 no chromium or oxygen was detected. From the sputter rate calibration this palladium-rich layer was found to be 1000 nm thick. At point B the interface between the palladium-rich layer and the oxide-rich layer was reached. At this palladium/oxide interface the palladium concentration decreased rapidly and the oxygen concentration increased as the oxide layer was exposed. Along with the oxygen increase the chromium concentration increased from essentially the noise level to slightly less than its bulk value. After another 2500 to 3000 nm of sputtering the oxygen concentration decreased while the palladium and chromium concentrations reached their bulk values. At this oxide/bulk interface, marked point C in figure 8, the oxide-rich layer was etched away. The depth from point B to point C was used to measure the oxide layer thickness of 3000 nm. The bulk alloy composition was calculated from the steady-state profile data and found to be 70 at.% palladium and 30 at.% chromium. The discrepancy between the bulk concentration values obtained from these profile data and the actual alloy composition was attributed to the relatively high noise levels present in the data and to the lack of standards, which prevented calculation of more precise sensitivity factors.

In an attempt to compare oxidation rates at different temperatures and hold times, the depths from the surface to the palladium/oxide and oxide/bulk interfaces were plotted as a function of annealing temperature. The position at which the palladium/oxide interface occurred was taken as the point where the palladium concentration rapidly decreased and the oxygen concentration rapidly increased (point B in fig. 8). The position at which the oxide/bulk interface occurred was taken as the point where the palladium concentration rapidly increased to its bulk value and the oxygen concentration rapidly decreased to the noise level (point C in fig. 8). These positions were determined somewhat subjectively and are therefore only approximate. The points B and C were chosen for each depth profile and the results were plotted. Figures 9(a) and (b) are the results for the wires annealed in air for 5 and 20 hr, respectively. The straight lines are linear least-squares fits to the data. Straight lines were chosen only because they represented the simplest possible dependence. In figure 9 the zero on the Y axis represents the wire surface. At any one temperature the depth from the surface to the palladium/oxide interface is the thickness of the palladium-rich layer, and the depth from the palladium/oxide interface to the oxide/bulk interface is the thickness of the oxide-rich layer. For both the 5- and 20-hr anneals the palladium-rich layer thickened with increasing temperature as evidenced by the upward slope of the line through the palladium/oxide interface points, but the thickness of the oxide-rich layer (the difference between the curves) remained roughly constant over the temperature ranges studied.

Long sputter times were required to sputter through the relatively thick palladium and oxide layers on the air-annealed samples. As a result, sputtering artifacts, such as severe cone formation, occurred. The formation of these artifacts as sputtering progressed can be seen in figure 10, which shows SED images recorded at various sputter depths for a wire annealed in air at 750 °C for 20 hr. These sputtering artifacts contributed to the uncertainty in the exact location of the interfaces and to the scatter observed in figure 9. In addition, the interfaces were by no means planar or sharp. The combination of the sputtering artifacts and the broad, nonplanar interfaces could have resulted in significant variations in the thickness measurements. The relatively poor signal-to-noise ratio of the depth profiles, primarily due to instrumental problems (as shown in fig. 8), further contributed to the scatter observed in figure 9.

Line scans.—Upon examining the wires that had been depth profiled, it was found that the heavy sputtering had ion milled the wires to a large extent and that in some areas this ion milling had exposed cross sections of the layered structures of the wires. Figure 11 schematically illustrates the geometry of these ion-milled sections. By recording Auger line scans across the revealed exposed layers, information similar to that obtained from the depth profiles could be recorded. In figure 11, as the electron beam was scanned from point D to point A, the Auger peak-to-peak intensities for palladium, chromium, and oxygen were recorded as a function of position. The y-axis is the peak-to-peak intensity relative to the baseline.

Three such line scans were taken on a wire that was annealed in air at 750 °C for 20 hr, after it had been sputtered for 13 hr. An SED image of the wire is shown in figure 12. The lines labeled 1, 2, and 3 correspond to the three different line scans. Figure 13 was recorded at the line marked 1 in figure 12. The 0-μm position of figure 13 corresponds to point D in figure 11 and the top of figure 12. Here, at point D in the bulk material the oxygen signal was near the noise level, but strong signals from palladium and chromium were recorded. As the beam was scanned across the wire, the first layer to be encountered after the bulk material was the oxide-rich layer. The interface between the bulk material and the oxide-rich layer is labeled C in the figures. As the beam scanned across the oxide-rich layer, the signals from oxygen and chromium became strong relative to the palladium signal, suggesting that this layer may contain Cr_2O_3, which is the most stable oxide of chromium. The next layer to be encountered was the palladium-rich layer. The interface between the oxide-rich layer and the palladium-rich layer is labeled B in the figures. A relatively strong signal from palladium was seen between points B and A in the figures. The decrease in the palladium signal at point A represented the edge of the wire. The electron beam then continued to scan past point A and off the wire. The increase in the chromium signal past the edge of the wire was due to chromium in the stainless steel sample mount. It must be remembered that the sputtering did not result in a true cross section through the center of the wire and that figure 11 is a much simplified schematic. Nevertheless, the line scans confirmed the results seen in the depth profiles—that the oxidized wires had a layered structure with a palladium-rich layer on the surface that was above an oxide-rich layer which in turn was above the bulk material.

Chemical maps of cross-sectioned ribbon. — In order to obtain data free from sputtering artifacts, a cross section of a PdCr ribbon was analyzed. Preparation of this sample is described in the Experimental Procedure section. Figure 14 shows an SED image along with palladium, chromium, and oxygen elemental maps of a cross section of a ribbon annealed in air at 800 °C for 16 hr. At the extreme left of the SED image was the plastic material in which the ribbon was mounted. Moving right, the dark, approximately vertical line was a gap where the plastic had pulled away from the ribbon. Next was the layered surface of the ribbon. Finally, the wide, dark-gray band in the center was the bulk PdCr alloy. On the right side of the SED image, at the other surface of the ribbon, the sequence repeated in reverse order.

In contrast to the heavily sputtered wire, this ribbon represented a true cross section that was prepared by mechanical cutting and polishing (see Experimental Procedure section). A small amount of sputtering (~25 nm) had been done on the cross section in order to remove the layer of gold that provided electrical conduction across the plastic mounting material. This sputtering was, however, much less than what the heavily sputtered wire was subjected to, and therefore no sputtering artifacts were noticed. In order to acquire an elemental map, the electron beam was slowly rastered across the area shown in figure 14(a) while the Auger peak intensity for a particular element was recorded. The peak intensity data were then converted to brightness levels. The resulting elemental map showed the concentration of the element, with white areas representing high concentrations and dark areas representing low concentrations. This rastering and recording sequence was repeated for each elemental map.

The elemental maps showed the same layered structure revealed by the depth profiles and line scans of the wires. Figure 14(b) is the palladium elemental map. At the surface of the ribbon (running approximately

vertically in fig. 14(b)) a thin, uneven, bright line was seen. Because this layer was bright on the palladium elemental map but dark on the chromium and oxygen elemental maps, it must have been composed of metallic palladium. Although this palladium-rich layer was uneven in thickness, the interface between it and the next deeper layer was nearly planar.

Beneath the palladium-rich layer was the oxide-rich layer. This layer was best seen in the oxygen elemental map (fig. 14(d)) where it showed up as bright lines near either surface of the ribbon. Because this layer showed a slight enrichment in chromium (fig. 14(c)) and was relatively devoid of palladium (fig. 14(b)), it probably consisted primarily of Cr_2O_3. Although the interface between the palladium-rich layer and the oxide-rich layer was nearly planar, the interface between the oxide-rich layer and the bulk material was rough. The bulk material showed up as wide, relatively bright bands running from top to bottom in the center of the palladium and chromium elemental maps. On the oxygen elemental map the bulk material appeared as a dark gray. The reason that this area was not black on the oxygen elemental map may be that there was some interference from the chromium Auger lines, which lie near in energy to the oxygen Auger line. Such interference could have resulted in a nonzero peak intensity being recorded for oxygen when in fact no oxygen was present.

Two other features were best seen on the palladium elemental map. The first was small dark spots, which were seen primarily near the center of the ribbon. Close examination showed that these spots were also dark on the chromium and oxygen elemental maps. These small spots were areas where the gold, which was deposited to provide electrical conduction, had not been completely removed by sputtering. The second feature was areas, in the bulk material and generally elongated right to left, that showed slightly different levels of brightness. These areas were the grains of the bulk material. The differences in brightness were believed to be due to slightly different yields of secondary electrons from the different crystal faces and not to actual differences in elemental concentration.

From the appearances of the surfaces and the interfaces between the layers in the cross section, inferences concerning the relative diffusion rates of chromium and oxygen can be drawn. The growth of Cr_2O_3 on chromium is believed to occur by outward diffusion of chromium cations (ref. 6). However, as shown in figure 14 the growth appeared to be at the interface between the alloy and the oxide-rich layer because the original surface of the ribbon was believed to be much smoother and more like the interface between the palladium-rich layer and the oxide-rich layer. This observation suggested that oxygen diffusion through the oxide layer was faster than chromium diffusion through the oxide layer. This was supported by the work of Hulse et al. (ref. 7), who also concluded that oxygen is the major diffusing species in the oxidation of PdCr. Oxidation along grain boundaries could, however, have been responsible for the appearance of the cross sections, and further study is required to determine the growth mechanism unambiguously.

Oxidation and segregation at grain boundaries.—In addition to the maps acquired on the cross section, elemental maps were also acquired on samples after they had been sputtered for depth profiling. Because the intensity of the argon ion beam that was used for sputtering fell off gradually away from the center of the beam, the resulting crater had broad, slowly sloping sides. Away from the center of the crater the depth to which the area had been sputtered gradually decreased. By acquiring elemental maps at different distances from the crater center, one could, in effect, determine the distribution of the various elements at various sputter depths.

Figure 15 shows postsputter AES elemental maps and an SED image that were recorded on the crater side walls for a wire annealed at 800 °C in air for 20 hr and sputtered for 13 hr. As shown schematically in figure 16, the area had been sputtered to approximately the interface between the oxide-rich layer and the bulk alloy; that is, both the palladium-rich layer and the oxide-rich layer had been largely sputtered away. The maps showed that, in addition to the layers seen on the surface, the layered structure extended

down the grain boundaries and partially surrounded the grains (fig. 16). The grains were easily seen on the palladium elemental map (fig. 15(b)) as gray areas outlined in black. The gray was the bulk PdCr that had been exposed by the sputtering. The black areas surrounding the grains on the palladium elemental map were bright in the chromium and oxygen elemental maps (figs. 15(c) and (d)). These areas were identified as chromium oxide. Bright spots on the palladium elemental map were areas where the palladium-rich surface layer had not sputtered away. Thin thread-like regions of palladium (arrows) surrounded by oxide-rich material were seen along grain boundaries. These thin threads of palladium-rich material were to the grain boundaries what the palladium-rich surface layer was to the wire surfaces. From the grain boundary into the grain the same structure was seen: a palladium-rich layer, then an oxide-rich layer, and then the bulk material.

A palladium-rich surface layer has been seen on all air-annealed samples. This surface layer may have been associated with the oxidation of chromium because, in general, no palladium layer has been observed on the vacuum-annealed samples. Metallic surface layers are sometimes observed to form when certain alloys undergo internal oxidation (ref. 8). In many ways, PdCr is similar to alloys that exhibit internal oxidation (refs. 9 and 10). Internal oxidation usually occurs in dilute solid-solution alloys composed of a relatively noble metal, such as palladium, and a small amount of a less noble metal, such as chromium. The more noble metal must exhibit a significant solubility and diffusivity for atomic oxygen. Although some disagreement exists (refs. 11 and 12), most researchers believe that the solubility and diffusivity of oxygen in palladium is relatively high (refs. 13 to 15). The percentage of the less noble metal must also be low enough to prevent an external scale from forming. Palladium containing 0.2% chromium is known to oxidize internally (ref. 10). However, because no evidence of internal oxidation, other than the metallic palladium surface layer, was detected in the present study, it may be concluded that the concentration of chromium in PdCr (13 wt%) was sufficiently high that an external oxide scale was formed before internal oxidation could have occurred. Oxidation along grain boundaries, which was evident on wire samples (fig. 15), could also have been responsible for the appearance of the ribbon cross section. The metallic palladium along the grain boundaries could have provided a path for oxygen diffusion and promoted grain boundary oxidation of chromium. Further study of the initial stages of the oxidation would help to clarify this point.

SUMMARY OF RESULTS

From the results obtained during these limited annealing studies the following observations regarding the oxidation effects of PdCr were made:

1. After air annealing at temperatures between 550 and 1000 °C, both ribbon and wire specimens exhibited similar chemical behavior, including palladium segregation to the surface, forming a palladium-rich layer up to several micrometers thick after five or more hours of thermal treatment, and the development of a several-micrometer-thick, palladium-deficient, oxide layer beneath the palladium-rich region.

2. Auger electron spectroscopy maps indicated that in the oxidation process oxygen was associated only with chromium and was concentrated near the grain boundaries and that at the grain boundaries a palladium-rich zone was detected with essentially no chromium or oxygen present.

3. Vacuum annealing did not produce the significant segregation that was detected after the air-annealing treatment.

4. Aluminum precipitates were observed on the surfaces of wire samples that were annealed in vacuum at temperatures above 700 °C.

5. The surface roughness of all samples heated in air increased with increasing temperature. For the depth profiles this surface roughness will influence the interpretation of the exact position of the interface between each layer.

CONCLUSIONS

The results of this study show that PdCr, as a fine wire or ribbon, does oxidize under the conditions studied. An understanding of the oxidation mechanism may lead to processing methods that can increase the operating time and/or temperature limit of this material as a sensor element.

Although the oxidation mechanism has been found to be complex, several steps of the oxidation process may be theorized from this study. First, oxygen reacts with chromium near the grain boundary, displacing palladium at this site. Palladium migrates along the grain boundary to the alloy surface. This palladium-rich surface layer may then act as a pathway for rapid oxygen diffusion farther into the alloy.

In addition to the palladium segregation, aluminum, most likely originating as an impurity from the alloy processing, migrates to the surface of the wires and ribbons at temperatures above 700 °C. Aluminum, which is an oxygen getter, may also contribute to the oxidation mechanism.

In order to control the oxidation, one can suggest the following steps to investigate in future studies:

1. Attempt to suppress the palladium segregation by coating with an oxygen diffusion barrier material.

2. Alter the grain boundary structure of the material by using a sputter-deposited, thin-film alloy sensor or by developing a pretreatment process for the wires, such as changing the cold working or annealing parameters.

3. Investigate the effect that impurities, such as aluminum, have on the oxidation.

REFERENCES

1. Hulse, C.O.; Bailey, R.S.; and Lemkey, F.D.: High Temperature Static Strain Gage Alloy Development Program. NASA CR–174833, 1985.

2. Anderson, W.L.; and Grant, H.P.: High Temperature Strain Gage Technology for Hypersonic Aircraft Development Applications. NASA CR–189101, 1992.

3. Zeller, M.V.; and Lei, J.F.: Surface Analysis Studies of the Oxidation of PdCr Strain Gage Material. Proceedings of the 177th Electrochemical Society Meeting, Vol. 90–1, Electrochemical Society, Pennington, NJ, 1990, ECS Abstract No. 934, p. 1318.

4. Lei, J.F.: A Resistance Strain Gage With Repeatable and Cancellable Apparent Strain for Use to 800 °C. NASA CR–185256, 1990.

5. Davis, L.E., et al.: Handbook of Auger Electron Spectroscopy. Physical Electronics Industries, Inc., Eden Prairie, MN, 1976.

6. Skeldon, M.; Calvert, J.M.; and Lees, D.G.: An Investigation of the Growth-Mechanism of Cr_2O_3 on Pure Chromium in 1-atm Oxygen at 950 °C. Oxid. Met., vol. 28, 1987, pp. 109–125.

7. Hulse, C.O., et al.: High Temperature Static Strain Gage Development Contract. NASA CR–180811, 1986.

8. Mackert, J.R., Jr.: Metallic Surface Layers Deposited by Diffusional Creep During Internal Oxidation. Metall. Trans. A: Phys. Metall. Mater. Sci., vol. 17A, 1986, pp. 746–749.

9. Rapp, R.A.: Kinetics, Microstructures and Mechanism of Internal Oxidation—Its Effect and Prevention in High Temperature Alloy Oxidation. Corrosion, vol. 21, 1965, pp. 382–400.

10. Guruswamy, S.M., et al.: Internal Oxidation of Ag-In Alloys: Stress Relief and the Influence of Imposed Strain. Oxid. Met., vol. 26, 1986, pp. 77–100.

11. Chaston, J.C.: Reactions of Oxygen With the Platinum Metals III—The Oxidation of Palladium. Platinum Met. Rev., vol. 9, 1965, pp. 126–129.

12. Park, J.-W.; and Altstetter, C.J.: The Diffusivity and Solubility of Oxygen in Solid Palladium. Scr. Metall., vol. 19, 1985, pp. 1481–1485.

13. Raub, E.; and Plate, W.: Über das Verhalten der Edelmetalle und ihrer Legierungen zu Sauerstoff bei hoher Temperatur im festen Zustand. Z. Metall., vol. 48, 1957, pp. 529–539.

14. Krier, C.A.; and Jaffee, R.I.: Oxidation of the Platinum-Group Metals. J. Less-Common Met., vol. 5, 1963, pp. 411–431.

15. Campbell, C.T.; Foyt, D.C.; and White, J.M.: Oxygen Penetration into the Bulk of Palladium. J. Phys. Chem., vol. 81, 1977, pp. 491–494.

BIBLIOGRAPHY

Palladium

Alcock, C.B.; and Hooper, G.W.: Thermodynamics of the Gaseous Oxides of the Platinum-Group Metals. Proc. R. Soc. London A, vol. 254A, 1960, pp. 551–561.

Baird, R.J.; Graham, G.W.; and Weber, W.H.: $PdRhO_2$ Formation During the Air Oxidation of a Pd-15Rh Alloy. Oxid. Met., vol. 29, no. 5/6, 1988, pp. 435–443.

Bell, W.E.; Inyard, R.E.; and Tagami, M.: Dissociation of Palladium Oxide. J. Phys. Chem., vol. 70, no. 11, Nov. 1966, pp. 3735–3736.

Campbell, C.T.; Foyt, D.C.; and White, J.M.: Oxygen Penetration Into the Bulk of Palladium. J. Phys. Chem., vol. 81, no. 5, May 1977, pp. 491–494.

Chaston, J.C.: Reactions of Oxygen With the Platinum Metals III—The Oxidation of Palladium. Platinum Met. Rev., vol. 9, 1965, pp. 126–129.

Darling, A.S.: Some Properties and Applications of the Platinum-Group Metals. Int. Met. Rev., vol. 18, 1973, pp. 91–122.

Dreger, L.H.; and Margrave, J.L.: Vapor Pressures of Platinum Metals. I. Palladium and Platinum, J. Phys. Chem., vol. 64, no. 9, Sept. 1960, pp. 1323–1324.

Graham, G.W., et al.: High-Temperature Oxidation of Pt-45Pd-10Rh. Oxid. Met., vol. 29, no. 5/6, 1988, pp. 487–497.

Higgins, P.K.; and Munir, Z.A.: Modification of the Sintering Kinetics of Palladium by a Surface Oxide. Metall. Trans. B, vol. 12B, no. 3, Sept. 1981, pp. 589–594.

Krier, C.A.; and Jaffee, R.I.: Oxidation of the Platinum-Group Metals. J. Less-Common Met., vol. 5, 1963, pp. 411–431.

Lee, D.-B.; and Simkovich, G.: Oxidation of Mo-W-Cr-Pd Alloys. J. Less-Common Met., vol. 163, 1990, pp. 51–62.

Lee, D.-B.; and Simkovich, G.: Oxidation Resistant Mo-W-Cr-Pd Alloys With Palladium Coatings. J. Less-Common Met., vol. 169, 1991, pp. 19–23.

Legare, P., et al.: Interaction of Oxygen and Hydrogen With Palladium. Surf. Sci., vol. 107, no. 2–3, 1981, pp. 533–546.

Livey, D.T.: The High Temperature Stability of Oxides and Sulfides. J. Less-Common Met., vol. 1, 1959, pp. 145–151.

Munir, Z.A.; and Coombs, P.G.: The Oxidation-Reduction Kinetics of Palladium Powder. Metall. Trans. B, vol. 14B, no. 1, Mar. 1983, pp. 95–99.

Park, J.-W.; and Altstetter, C.J.: The Diffusivity and Solubility of Oxygen in Solid Palladium. Scr. Metall., vol. 19, no. 12, 1985, pp. 1481–1485.

Raub, E.: Metals and Alloys of the Platinum Group. J. Less-Common Met., vol. 1, 1959, pp. 3–18.

Raub, E.; and Plate, W.: Über das Verhalten der Edelmetalle und ihrer Legierungen zu Sauerstoff bei hoher Temperatur im festen Zustand. Z. Metall., vol. 48, 1957, pp. 529–539.

Rubel, M., et al.: Oxygen Generated Platinum, Rhodium and Palladium Volatile Losses From Pure Metals and Their Alloys. J. Less-Common Met., vol. 125, 1986, pp. 7–24.

Sandler, Y.L.; and Durigon, D.D.: The Low-Temperature Isotopic Oxygen Equilibration on Oxidized Palladium. J. Phys. Chem., vol. 73, no. 7, July 1969, pp. 2392–2396.

Tomashov, N.D. (B.H. Tytell, I. Geld, and H.S. Preiser, transl.): Theory of Corrosion and Protection of Metals: The Science of Corrosion, Macmillan Company, New York, 1966, pp. 8, 9, 42, 43, 651.

Chromium

Atkinson, H.V.: A Review of the Role of Short-Circuit Diffusion in the Oxidation of Nickel, Chromium, and Nickel-Chromium Alloys. Oxid. Met., vol. 24, no. 3/4, 1985, pp. 177–197.

Chu, W.F.; and Rahmel, A.: The Kinetics of the Reduction of Chromium Oxide by Hydrogen. Metall. Trans. B, vol. 10B, no. 3, Sept. 1979, pp. 401–407.

Kim, Y.-W.; and Belton, G.R.: The Thermodynamics of Volatilization of Chromic Oxide: Part I. The Species CrO_3 and CrO_2OH. Metall. Trans., vol. 5, no. 8, Aug. 1974, pp. 1811–1816.

Sano, N.; and Belton, G.R.: The Thermodynamics of Volatilization of Chromic Oxide: Part II. The Species CrO_2Cl_2. Metall. Trans., vol. 5, no. 10, Oct. 1974, pp. 2151–2154.

Skeldon, M.; Calvert, J.M.; and Lees, D.G.: An Investigation of the Growth Mechanism of Cr_2O_3 on Pure Chromium in 1 atm Oxygen at 950 °C. Oxid. Met., vol. 28, no. 1/2, 1987, pp. 109–125.

Wilms, G.R.; and Rea, T.W.: Atmospheric Contamination of Chromium and Its Effect on Mechanical Properties. J. Less-Common Met., vol. 1, 1959, pp. 152–156.

PdCr Phase Diagrams

Grube, G.; and Knabe, R.: Elektrische Leitfähigkeit und Zustandsdiagramm bei Binären Legierungen, Das System Palladium-Chrom. Z. Elektrochem., bd. 42, nr. 11, 1936, pp. 793–804.

Raub, E.; and Mahler, W.: Die Palladium-Chrom-Legierungen. Z. Metall., vol. 45, 1954, pp. 648–650.

Savitsky, E., et al. (I. Savin, transl.): Physical Metallurgy of Platinum Metals. Pergamon Press, New York, 1978, pp. 238, 242, 243.

Van Rijn, H.J.; Alberts, H.L.; and Smit, P.: On the Solubility of Palladium in Chromium. J. Less-Common Met., vol. 107, 1985, pp. L9–L11.

Vines, R.F.: The Platinum Metals and Their Alloys. The International Nickel Company, Inc., New York, 1941, pp. 102–104.

Waterstrat, R.M.: Analysis of Selected Alloys in the Systems Cr-Pd, Cr-Ru, V-Pd, and Ta-Pt. J. Less-Common Met., vol. 80, 1981, pp. P31–P36.

Oxidation

Arkharov, V.I., et al.: On the Mechanism of Chemical Diffusion in Solids and Its Application to Oxidation. Oxid. Met., vol. 3, no. 3, 1971, pp. 251–259.

Arkharov, V.I., et al.: Reply to J.D. Kuenzly's Discussion of 'On the Mechanism of Chemical Diffusion in Solids and Its Application to Oxidation.' Oxid. Met., vol. 3, no. 4, 1971, pp. 361–363.

Bailey, J.M.; and Ritchie, I.M.: An Electrochemical Analysis of Surface Control. Oxid. Met., vol. 30, no. 5/6, 1988, pp. 419–432.

Bailey, J.M.; and Ritchie, I.M.: Metal Oxidation: An Electrochemical Perspective. Oxid. Met., vol. 30, no. 5/6, 1988, pp. 405–418.

Chassagneux, E.; Soustelle, M.; and Thomas, G.: Kinetics of the Oxidation of Metals: Parallel Circuit for Point Defects Diffusion. Oxid. Met., vol. 27, no. 5/6, 1987, pp. 301–314.

Denis, A.; and Garcia, E.A.: Model to Simulate Parabolic Followed by Linear Oxidation Kinetics. Oxid. Met., vol. 29, no. 1/2, 1988, pp. 153–167.

Kuenzly, J.D.: Discussion of 'On the Mechanism of Chemical Diffusion in Solids and Its Application to Oxidation.' Oxid. Met., vol. 3, no. 4, 1971, pp. 357–359.

Lees, D.G.: On the Reasons for the Effects of Dispersions of Stable Oxides and Additions of Reactive Elements on the Adhesion and Growth-Mechanisms of Chromia and Alumina Scales—The 'Sulfur Effect.' Oxid. Met., vol. 27, no. 1/2, 1987, pp. 75–81.

Morin, F.; Beranger, G.; and Lacombe, P.: Limits of Application for Wagner's Oxidation Theory. Oxid. Met., vol. 4, no. 1, 1972, pp. 51–62.

Morin, F.; Beranger, G.; and Lacombe, P.: Rebuttal of the Discussion of 'Limits of Application for Wagner's Oxidation Theory.' Oxid. Met., vol. 7, no. 2, 1973, pp. 147–148.

Mrowec, S.; and Stoklosa, A.: Discussion of 'Limits of Application for Wagner's Oxidation Theory.' Oxid. Met., vol. 7, no. 2, 1973, pp. 141–145.

Rapp, R.A.: The High Temperature Oxidation of Metals Forming Cation-Diffusing Scales. Metall. Trans. A, vol. 15A, no. 5, May 1984, pp. 765–782.

van Loo, F.J.J., et al.: On the Layer Sequence and Morphology in Solid-State Displacement Reactions. Oxid. Met., vol. 22, no. 3/4, 1984, pp. 161–180.

Vedula, K.: Modeling of Transient and Steady-State Demixing of Oxide Solid Solutions in an Oxygen Chemical Potential Gradient. Oxid. Met., vol. 28, no. 1/2, 1987, pp. 99–108.

Wood, G.C.: High-Temperature Oxidation of Alloys. Oxid. Met., vol. 2, no. 1, 1970, pp. 11–57.

Young, D.J.; and Gesmundo, F.: Thermodynamics of Ionic Diffusion and Oxidation Rate Equations. Oxid. Met., vol. 29, no. 1/2, 1988, pp. 169–185.

Strain Gages

Bertodo, R.: Resistance Strain Gauges for the Measurement of Steady Strains at High Temperatures. Inst. Mech. Eng. Proc., Pt. A, vol. 178, no. 34, 1963–1964, pp. 907–926.

Bertodo, R.: High Temperature Strain Gauges for Turbo-Jet Components. Platinum Met. Rev., vol. 8, no. 4, Oct. 1964, pp. 128–130.

Brittain, J.O.; Geslin, D.; and Lei, J.F.: Elevated Temperature Strain Gages. Turbine Engine Hot Section Technology, 1985, NASA CP–2405, 1985, pp. 59–65.

Brittain, J.O.; Geslin, D.; and Lei, J.F.: Elevated Temperature Strain Gages. Turbine Engine Hot Section Technology, 1986, NASA CP–2444, 1986, pp. 69–84.

Easterling, K.E.: High Temperature Resistance Strain Gauges. Br. J. Appl. Phys., vol. 14, no. 1, 1963, pp. 79–84.

Englund, D.R.: The Dual Element Method of Strain Gauge Temperature Compensation. SEM, Fourth Annual Hostile Environments and High Temperature Measurements Conference Proceedings, Society for Experimental Mechanics, Inc., Bethel, CT, 1987, pp. 40–42.

Englund, D.R.: Progress on a PdCr Wire Strain Gage. Turbine Engine Hot Section Technology, 1987, NASA CP–2493, 1987, pp. 77–79.

Grant, H.P.; Anderson, W.L.; and Przybyszewski, J.S.: Rotating Tests of Advanced High Temperature Wire and Thin-Film Strain Gages. AIAA Paper 88–3146, July 1988, pp. 1–13.

Hobart, H.F.: Evaluation Results of the 700 °C Chinese Strain Gages for Gas Turbine Engine. NASA TM–86973, 1985, pp. 77–84.

Hobart, H.F.: The NASA Lewis Strain Gauge Laboratory—An Update. Turbine Engine Hot Section Technology, 1986, NASA CP–2444, 1986, pp. 91–96.

Hobart, H.F.; and Will, H.A.: The Lewis Strain Gauge Laboratory—Status and Plans. Turbine Engine Hot Section Technology, 1985, CP–2405, 1985, pp. 77–79.

Hulse, C.O., et al.: High Temperature Static Strain Gage Development Contract. NASA CR–180811, 1986.

Hulse, C.O., et al.: Development of a High Temperature Thin Film Static Strain Gage. Turbine Engine Hot Section Technology, 1987, NASA CP–2493, 1987, pp. 43–51.

Hulse, C.O.; Bailey, R.S.; and Grant, H.P.: The Development of a High Temperature Static Strain Gage System. Turbine Engine Hot Section Technology, 1985, NASA CP–2405, 1985, pp. 45–49.

Hulse, C.O.; Bailey, R.S.; and Grant, H.P.: Development of a High Temperature Static Strain Sensor. Turbine Engine Hot Section Technology, 1986, NASA CP–2444, 1986, pp. 85–90.

Hulse, C.O.; Bailey, R.S.; and Lemkey, F.D.: High Temperature Static Strain Gage Alloy Development Program. NASA CR–174833, 1985.

Lei, J.-F.: Development and Characterization of PdCr Temperature-Compensated Wire Resistance Strain Gage. NASA CR–185153, 1989, pp. 1–7.

Lei, J.-F.: A Resistance Strain Gage With Repeatable and Cancellable Apparent Strain for Use to 800 °C. NASA CR–185256, 1990, pp. 1–8.

Lei, J.-F.: The Apparent Strain Stability and Repeatability of a BCL3 Resistance Strain Gage. NASA CR–187056, 1991, pp. 1–9.

Lei, J.-F.; Mentor, J.; and Van Horn, H.J.: Influence of Rare Earth Oxide Addition on the Oxidation Behavior of PdCr Strain Gauge Material. Proceedings of the 177th Electrochemical Society Meeting, Vol. 90–1, Electrochemical Society, Pennington, NJ, 1990, ECS Abstract No. 933, p. 1317.

Lei, J.-F.; Shaarbaf, M.; and Brittain, J.O.: Elevated Temperature Strain Gages. Turbine Engine Hot Section Technology, 1987, NASA CP–2493, 1987, pp. 53–75.

Lei, J.-F.; and Williams, W.D.: PrCr Based High Temperature Static Strain Gage. AIAA Paper 90–5236, 1990.

Lemcoe, M.M.: Development of High Temperature Strain Gages. NASA CR–112241, 1973, pp. 1–103.

Lemcoe, M.M.: Valid Resistance Strain Gage Measurements to Temperatures Approaching 2000 °F: Can It Be Done? Presented at the Sensors Expo International Conference, Cleveland, OH, Sept. 12–14, 1989.

Ma, L.-C.; Wu, Z.-D.; and Zhao, L.-B.: Development of Temperature-Compensated Resistance Strain Gages for Use to 800 °C. International Conference on Experimental Mechanics, C. Li and L. Yang, eds., Science Press, Beijing, People's Republic of China, 1985, pp. 62–68.

Schabtach, C.; and Fehr, R.O.: Measurement of the Damping of Engineering Materials During Flexural Vibration at Elevated Temperatures. ASME Trans., vol. 66, 1944, pp. A86–A92.

Wu, T.-T.; Ma, L.-C.; and Zhao, L.-B.: Development of Temperature-Compensated Resistance Strain Gages for Use to 700 °C. Exp. Mech., vol. 21, Mar. 1981, pp. 117–123.

Zeller, M.V.; and Lei, J.-F.: Surface Analysis Studies of the Oxidation of PdCr Strain Gage Material. Proceedings of the 177th Electrochemical Society Meeting, Vol. 90–1, Pennington, NJ, 1990, ECS Abstract No. 934, p. 1318.

Internal Oxidation

Guruswamy, S., et al.: Internal Oxidation of Ag-In Alloys: Stress Relief and the Influence of Imposed Strain. Oxid. Met., vol. 26, no. 1/2, 1986, pp. 77–100.

Mackert, J.R., Jr.: Metallic Surface Layers Deposited by Diffusional Creep During Internal Oxidation. Metall. Trans. A, vol. 17A, no. 4, Apr. 1986, pp. 746–749.

Rapp, R.A.: Kinetics, Microstructures and Mechanism of Internal Oxidation—Its Effect and Prevention in High Temperature Alloy Oxidation. Corrosion, vol. 21, 1965, pp. 382–400.

Whittle, D.P.; El-Dahshan, M.E.; and Stringer, J.: The Oxidation Behavior of Cobalt-Base Alloys Containing Dispersed Oxides Formed by Internal Oxidation. Corros. Sci., vol. 17, 1977, pp. 879–891.

Miscellaneous

Bragg, W.L.; and Williams, E.J.: The Effect of Thermal Agitation on Atomic Arrangement in Alloys. Proc. R. Soc. London A, vol. 145A, 1934, pp. 699–730.

Taylor, A.; and Hinton, K.G.: A Study of Order-Disorder and Precipitation Phenomena in Nickel-Chromium Alloys. J. Inst. Met., vol. 81, 1953, pp. 169–180.

TABLE I.—SAMPLES USED FOR AES ANALYSIS

Annealing procedure			Material[a]	
Temperature, °C	Time, hr	Environment	Ribbon	Wire
550	5	Vacuum	•	•
	20	↓	•	•
650	5	↓	•	•
	20	↓	•	•
750	↓	↓	•	•
800	↓	↓	•	•
850	↓	↓	•	•
950	↓	↓	•	•
1000	↓	↓		•
550	5	Air	•	•
600	20	↓		•
650	5	↓		•
	20	↓		•
750	20	↓		•
800	20	↓	•	•
850	5	↓		•
950	5	↓	•	•

[a]A • indicates that a sample was analyzed by AES.

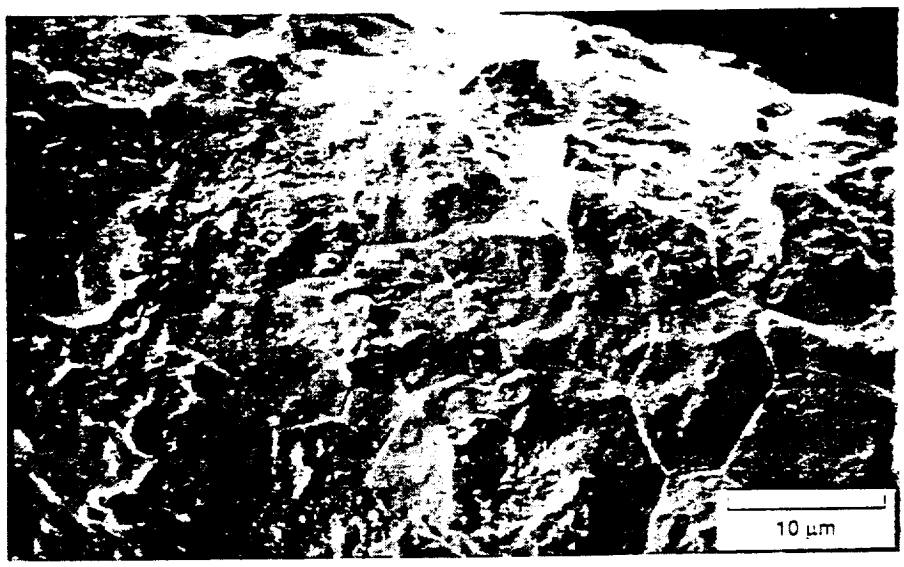

(a) 550 °C.

(b) 750 °C.

Figure 1.—SED images of PdCr wires annealed in vacuum at 550, 750, and 950 °C for 20 hr.

(c) 950 °C.

Figure 1.—Concluded.

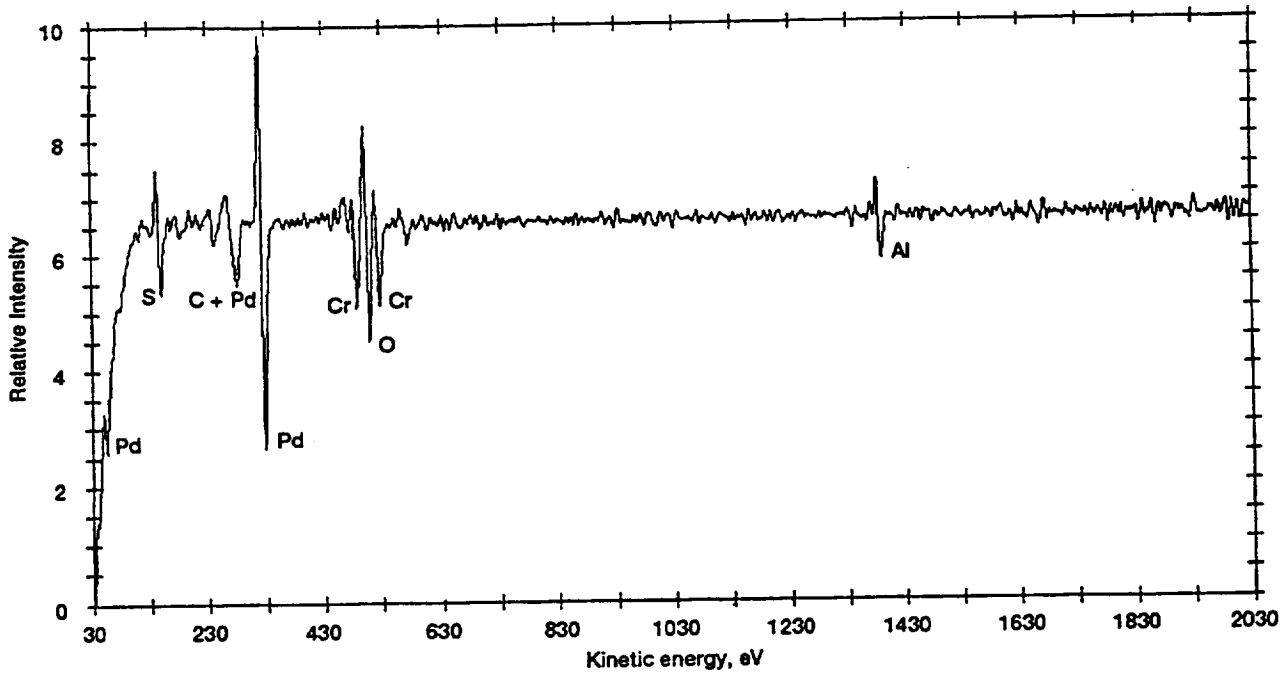

Figure 2.—AES survey scan of unsputtered PdCr wire annealed in vacuum at 800 °C for 20 hr. (The electron beam was focused onto a precipitate on the wire surface.)

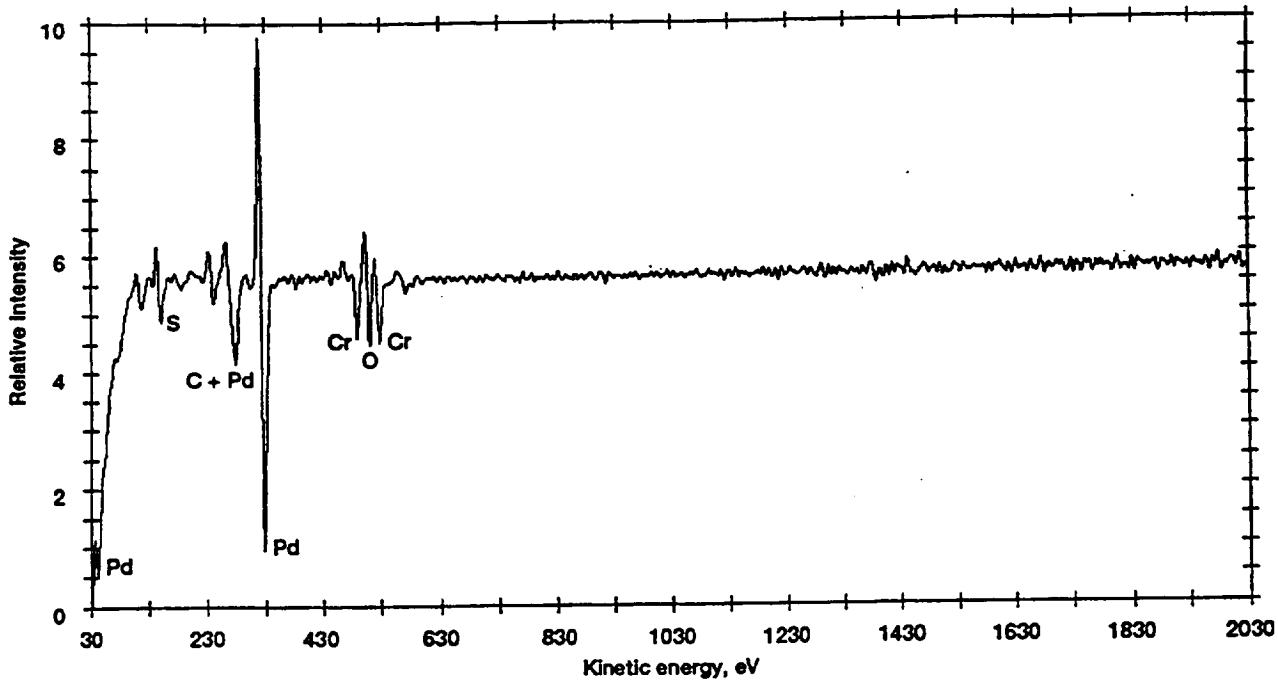

Figure 3.—AES survey scan of unsputtered PdCr wire annealed in vacuum at 1000 °C for 20 hr. (The electron beam was focused onto a featureless area of the wire.)

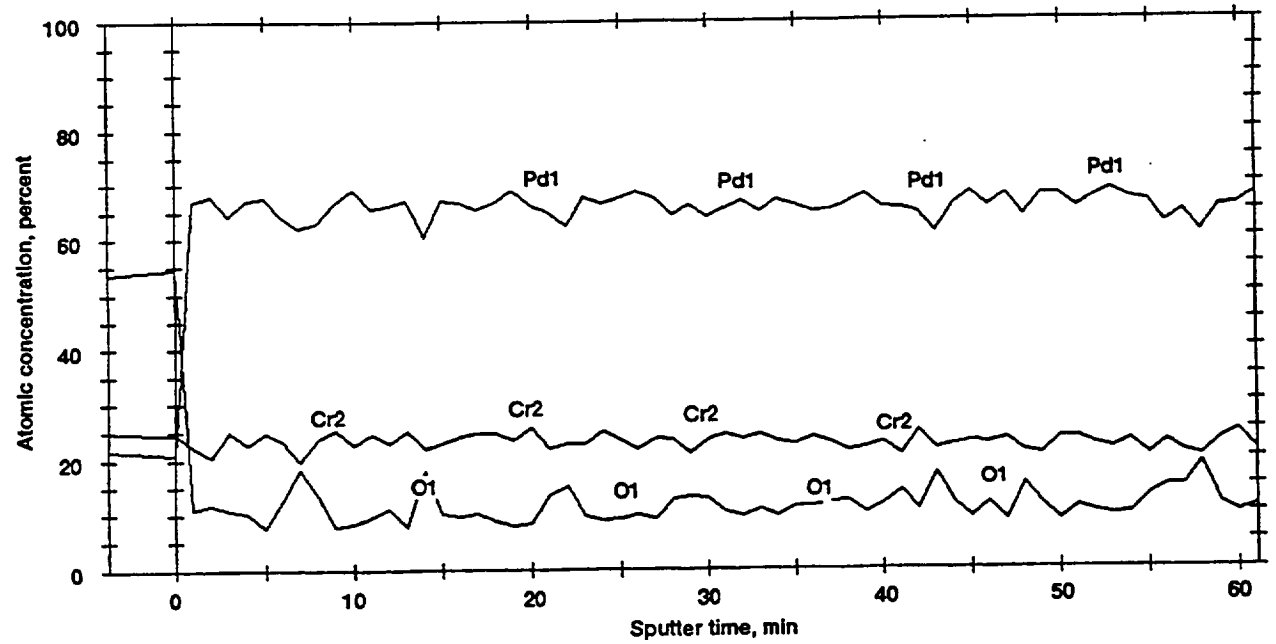

Figure 4.—AES depth profile of PdCr ribbon annealed in vacuum at 650 °C for 20 hr. Sputter rate, ~10 nm/min.

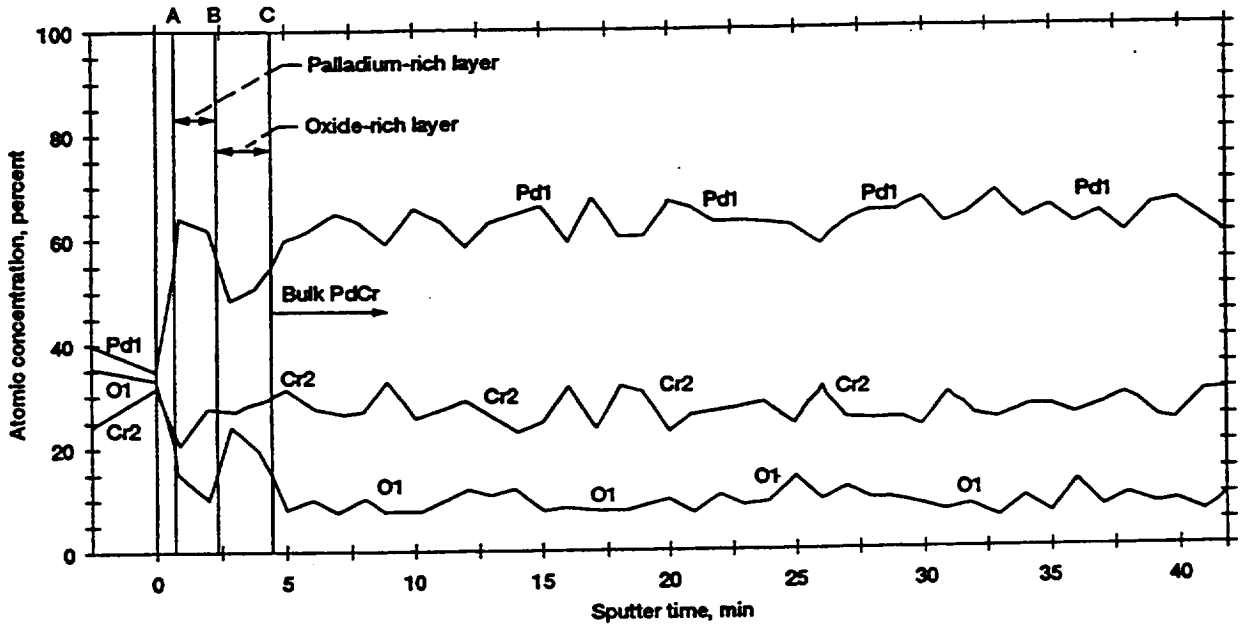

Figure 5.—AES depth profile of PdCr wire annealed in vacuum at 950 °C for 20 hr. (Between A and B a palladium-rich layer was observed, followed by an oxide-rich layer between B and C. The bulk PdCr was detected after C, or after 50 nm of surface had been removed.)

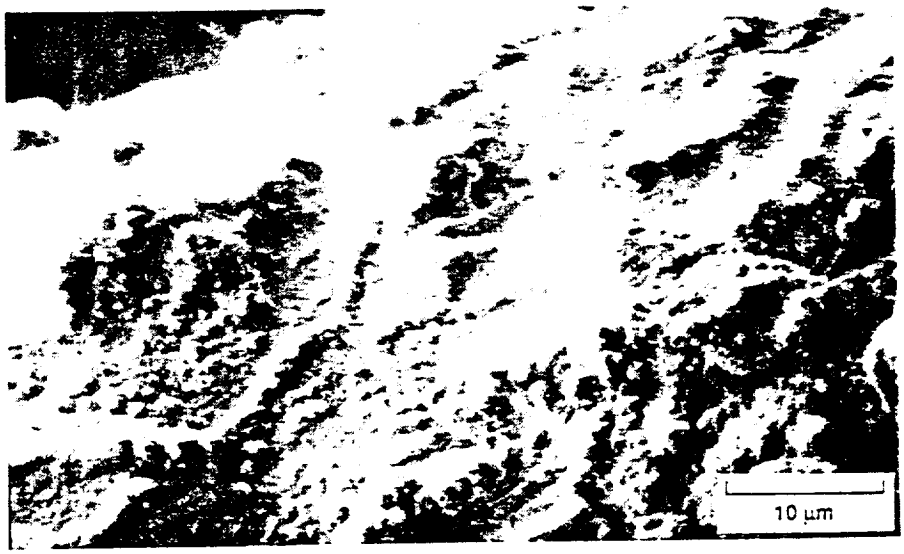

(a) 550 °C.

Figure 6.—SED images of PdCr wires annealed in air at 550, 750, and 800 °C for 20 hr. (Ridges are visible on the samples annealed below 800 °C, (a) and (b)).

(b) 750 °C.

(c) 800 °C.

Figure 6.—Concluded.

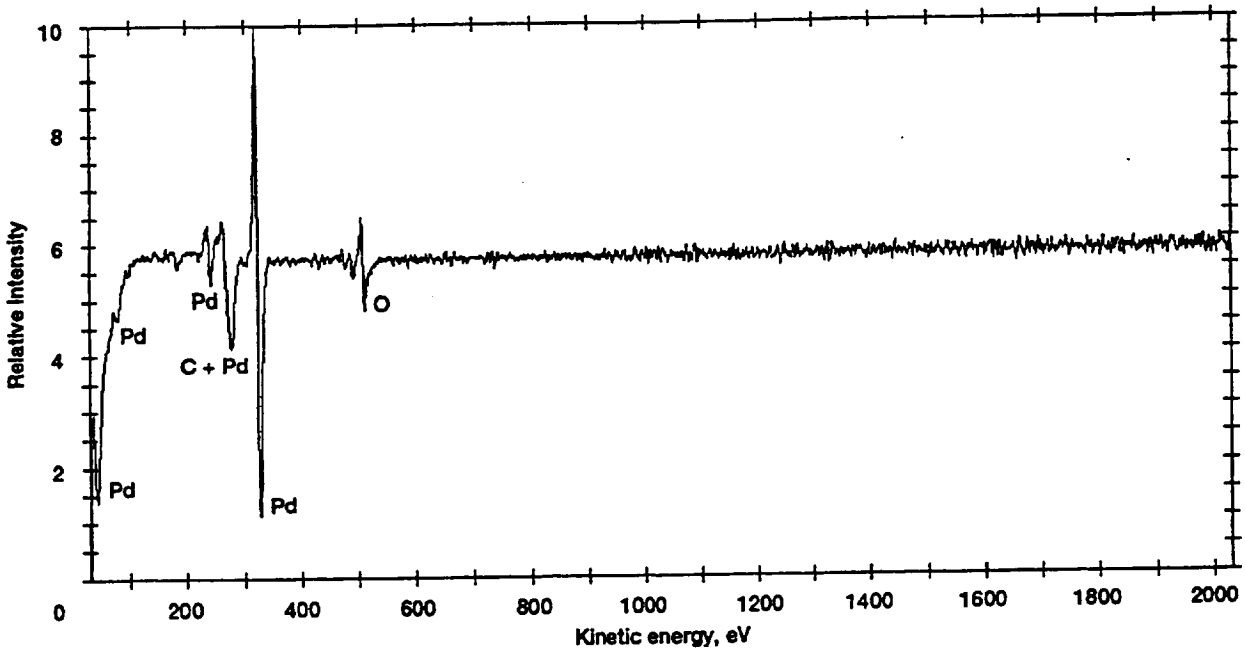

Figure 7.—AES survey scan of unsputtered PdCr wire annealed in air at 850 °C for 5 hr.

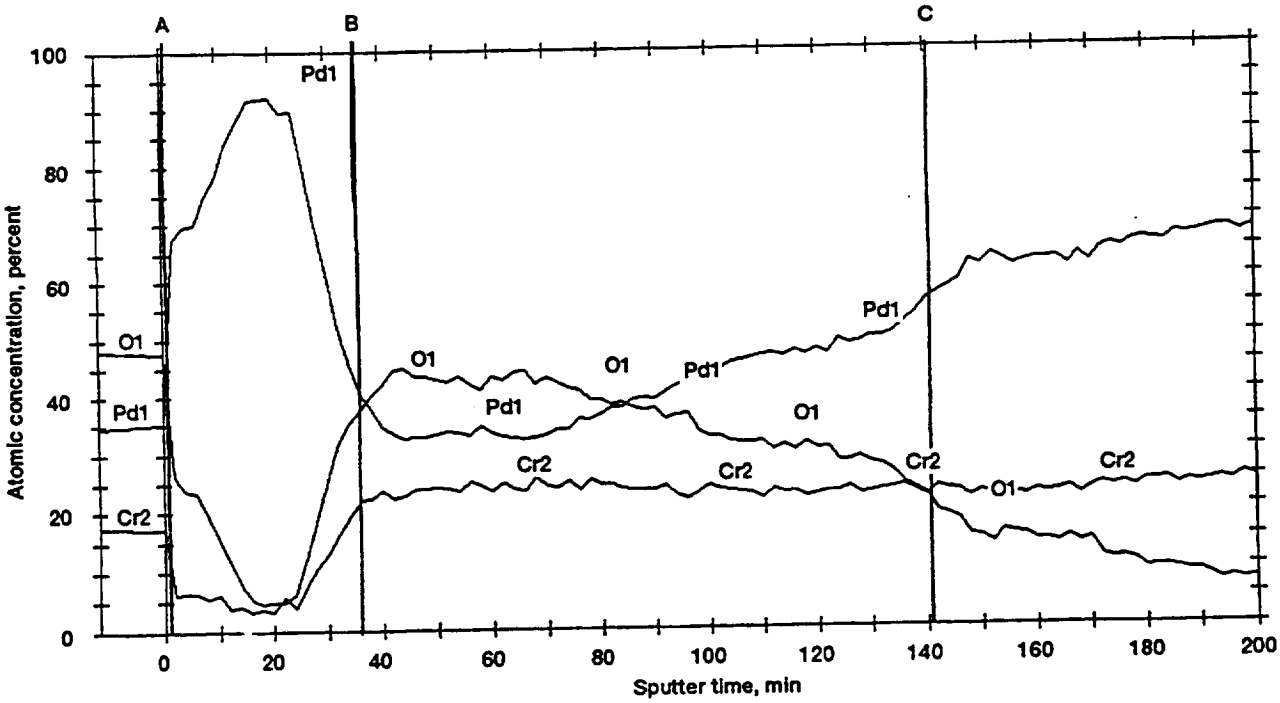

Figure 8.—AES depth profile of PdCr wire annealed in air at 600 °C for 20 hr. (Between A and B a palladium-rich layer was detected. Between B and C an oxide-rich layer was observed. To the right of point C the atomic concentrations were representative of the bulk material.)

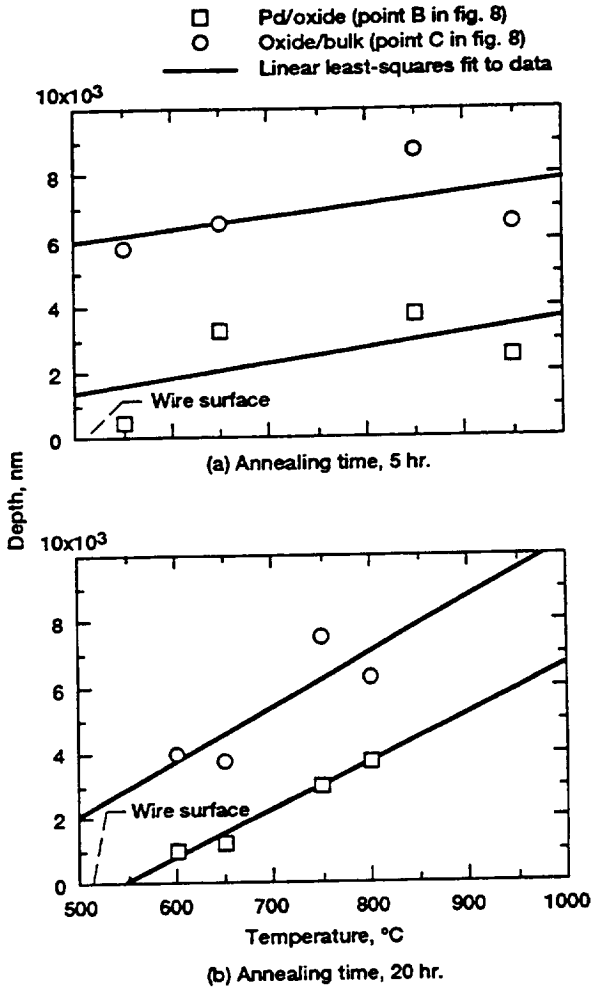

Figure 9.—Depth from surface to palladium/oxide interface and depth from surface to oxide/bulk interface as a function of anneal temperature for PdCr wires annealed in air for 5 and 20 hr.

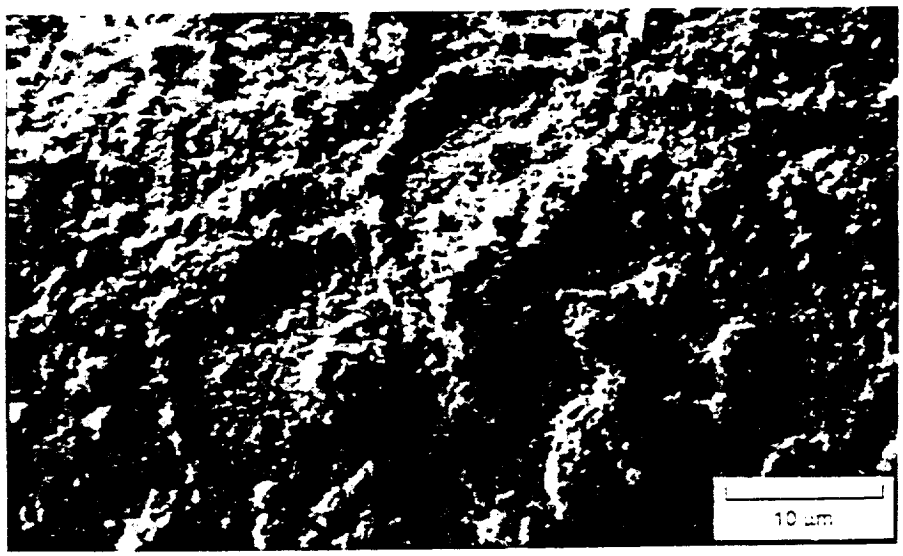

(a) Surface of unsputtered wire.

(b) Surface layers removed; oxidation visible along grain boundaries.

Figure 10.—Development of sputtering artifacts on PdCr wire annealed in air at 750 °C for 20 hr.

(c) Severe cone formation visible after 13 hr of sputtering.

Figure 10.—Concluded.

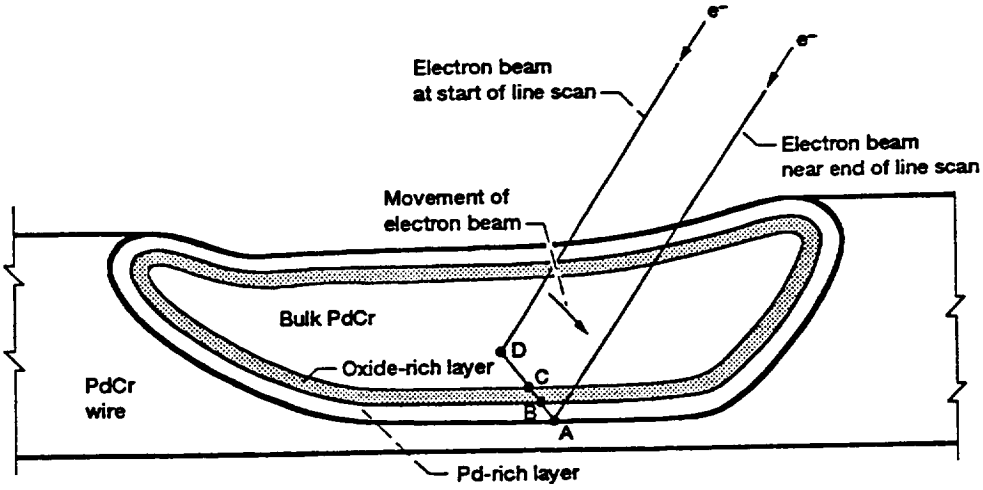

Figure 11.—Schematic drawing of ion-milled section of wire showing geometry of line scans. (The line scans began at point D in bulk material. The electron beam was then scanned across the layered structures of the wires, first crossing the interface between the bulk material and the oxide-rich layer (point C), then the interface between the oxide-rich layer and the palladium-rich layer (point B), and finally leaving the wire at point A.)

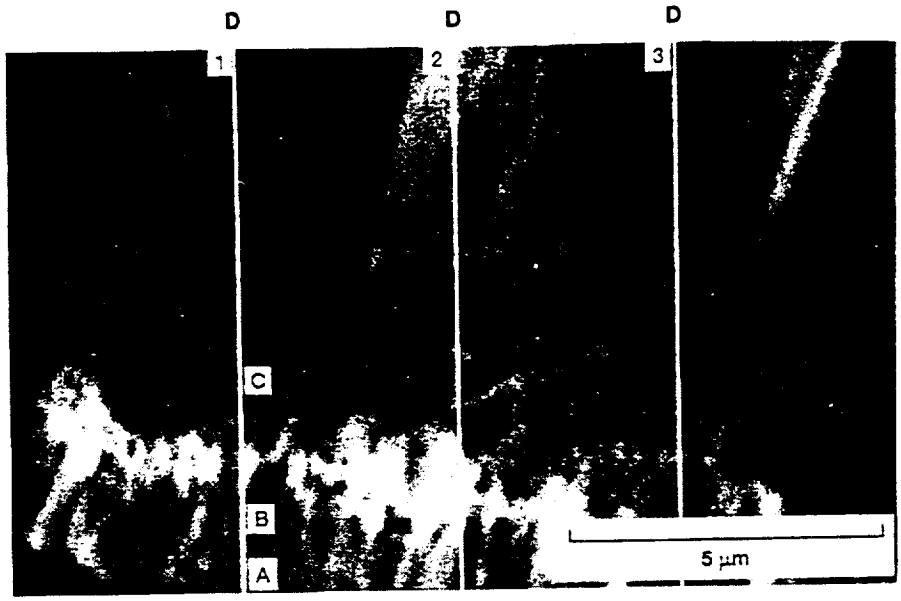

Figure 12.—SED image of wire annealed in air at 750 °C for 20 hr after being sputtered for 13 hr. (The vertical white lines labeled 1, 2, and 3 show where data were collected. Each scan began at point D. Point C is the approximate position of the interface between the bulk material and the oxide-rich layer. Point B is the approximate position of the interface between the oxide-rich layer and the palladium-rich layer. Point A is the edge of the wire.)

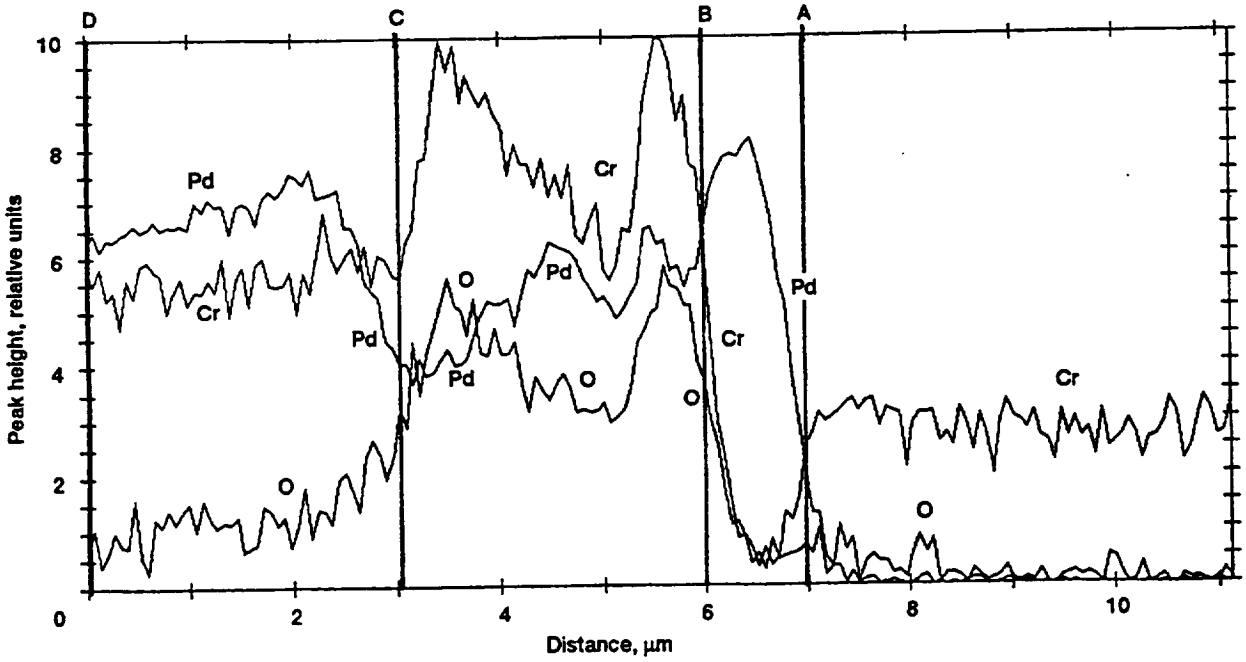

Figure 13.—AES line scan of PdCr wire annealed in air at 750 °C for 20 hr after being sputtered for 13 hr. (The A, B, C, and D designations refer to the labeled areas in figure 12.)

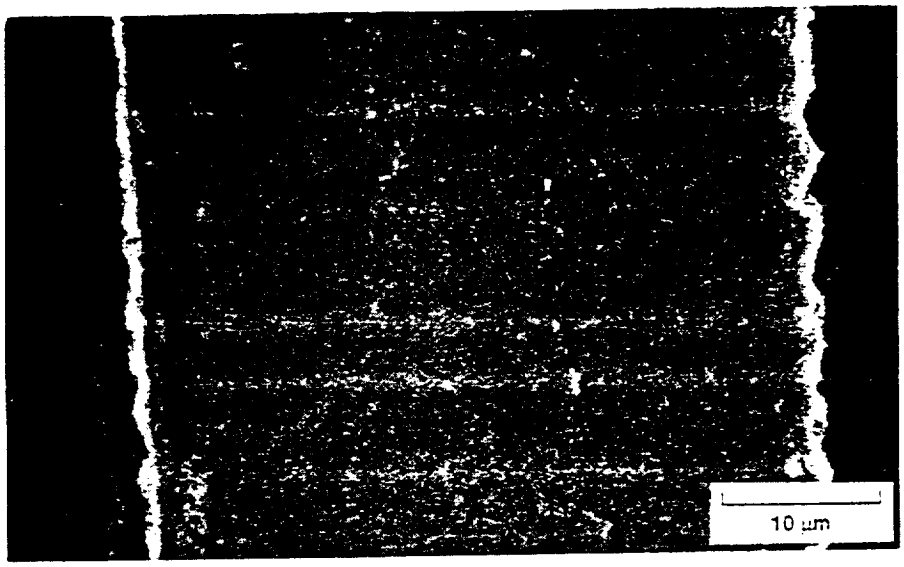

(a) SED image.

(b) Pd map.

Figure 14.—SED image along with palladium, chromium, and oxygen elemental maps of cross section of PdCr ribbon annealed in air at 800 °C for 16 hr. (On the elemental maps bright areas represent high concentrations of a particular element and dark areas low concentrations.)

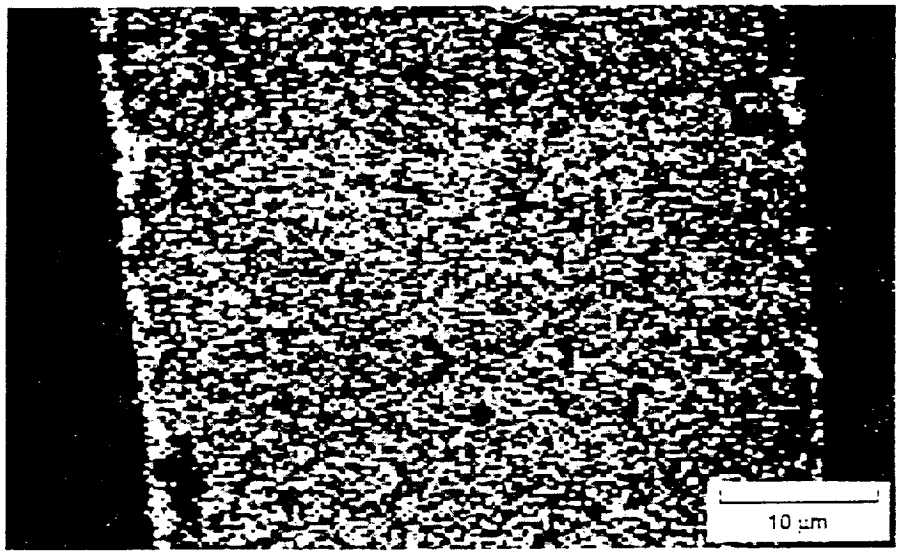

(c) Cr map.

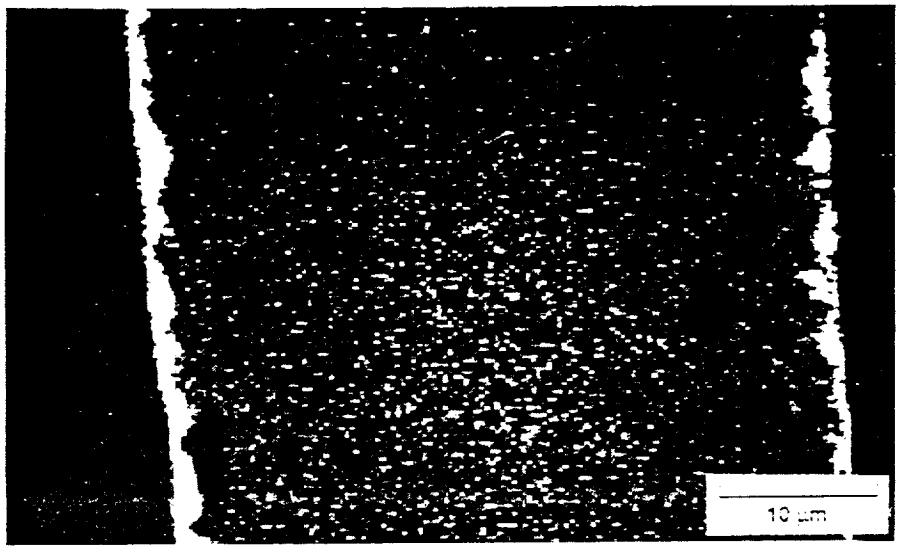

(d) O map.

Figure 14.—Concluded.

(a) SED image.

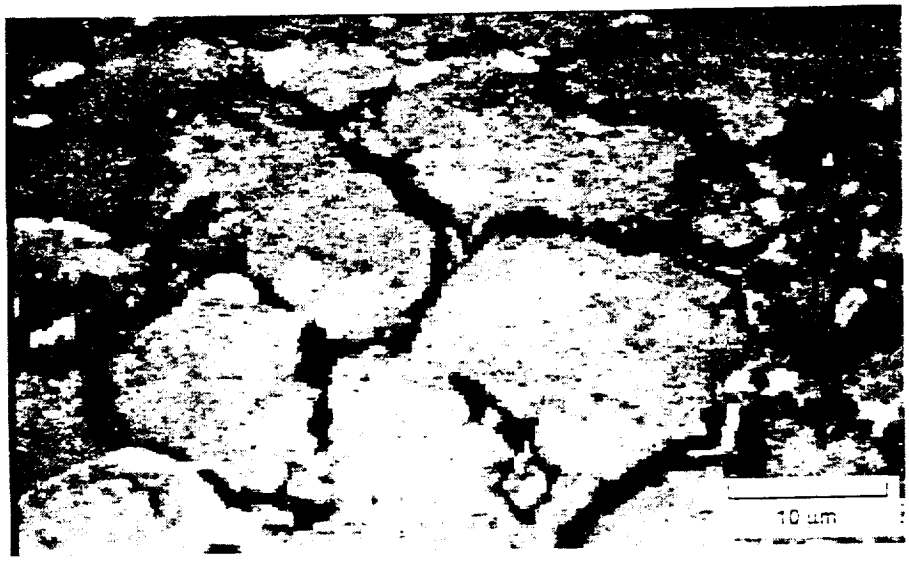

(b) Pd map.

Figure 15.—SED image along with palladium, chromium, and oxygen elemental maps of PdCr wire annealed in air at 800 °C for 20 hr. (This area had been sputtered to approximately the interface between the oxide-rich layer and the bulk material.)

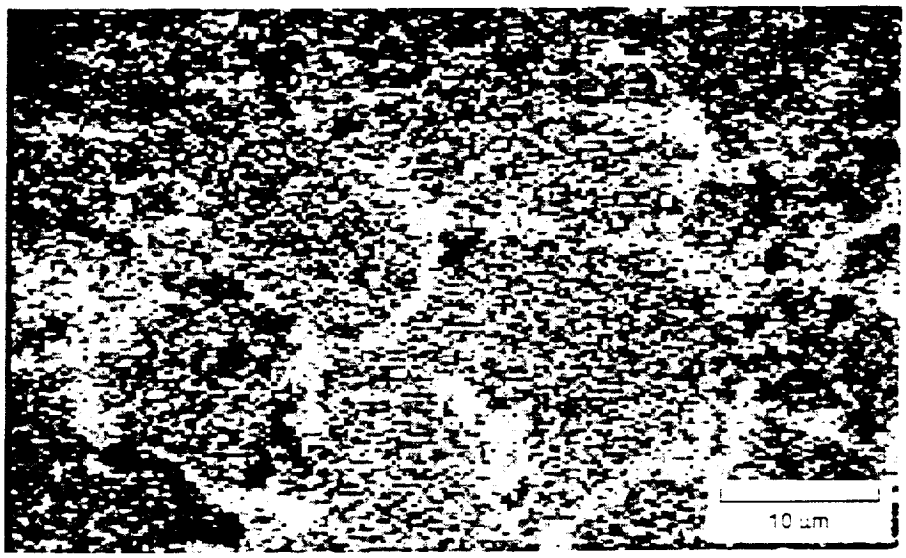

(c) Cr map.

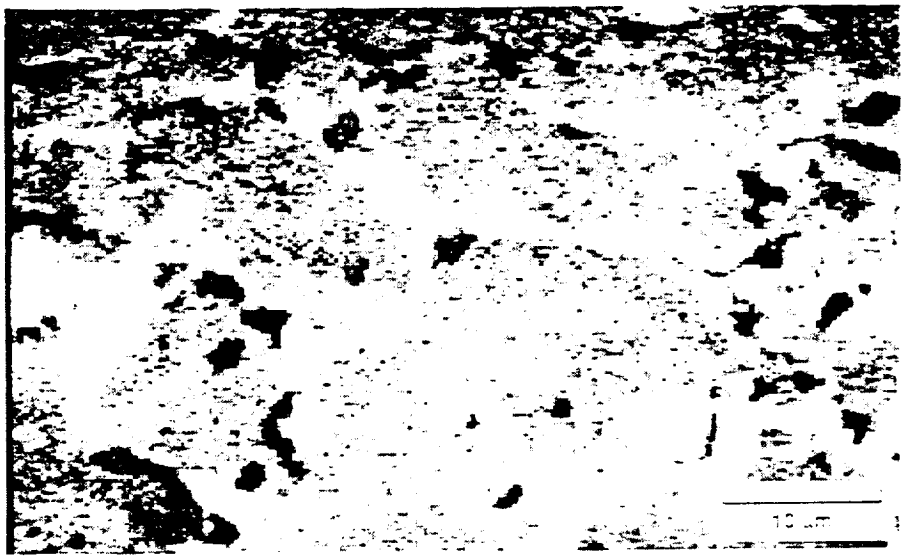

(d) O map.

Figure 15.—Concluded.

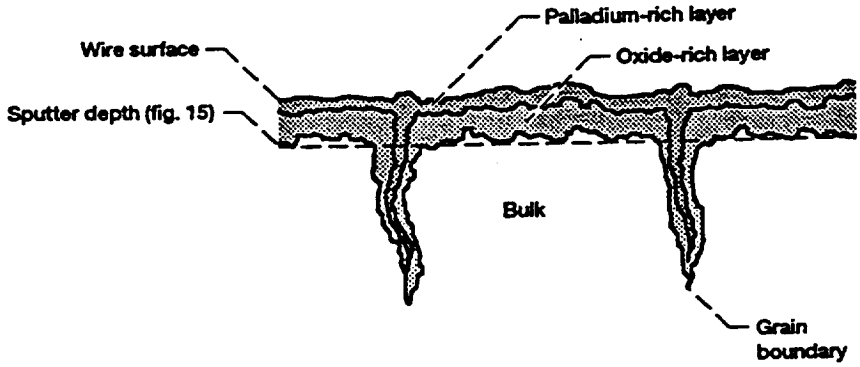

Figure 16.—Schematic cutaway view of PdCr wire after air annealing. (The dotted line shows the approximate depth to which the wire shown in figure 15 had been sputtered. The layered structure of the surface is seen to extend down the grain boundaries.)